

Uranium metallogeny in the North Flinders Ranges region of South Australia

Pierre-Alain Wülser

Department of Geology and Geophysics
Adelaide University

This thesis is submitted in the fulfilment of the requirements for the
degree of Doctor of Philosophy in the Faculty of Science, Adelaide
University

June 2009



Table of content

List of Figures	7
List of Tables & Appendix.....	10
Abstract	11
Declaration.....	12
Acknowledgments.....	13
GENERAL INTRODUCTION.....	14
ANALYTICAL TECHNIQUES.....	16
A.1 Heavy mineral and sample preparation.....	16
A.2 Zircon typology and morphology: principles.....	16
A.3 Chemical and isotopic composition analysis.....	17
A.3.1 Backscattered Scanning Electron microscope study.....	17
A.3.2 Electron microprobe analysis.....	17
A.3.3 Sulphide isotopes determination.....	19
A.3.4 U-Pb dating by laser-ablation ICPMS.....	19
A.3.5 Whole-rock analysis: Fe ²⁺ determination & XRF analysis.....	19
A.3.6 Trace element analysis by LA-ICPMS.....	19
PART ONE – The Sandstone-hosted Beverley Uranium Deposit.....	20
1 Introduction & Location.....	21
2 Geological setting.....	22
2.1 General geology.....	22
2.1.1 Cretaceous formations.....	22
2.1.2 Palaeocene to Oligocene (Eyre Formation, silcretes and ferricretes).....	23
2.1.3 Late Oligocene to Miocene (Namba, Neurodla and Etadunna formations).....	24
2.1.4 Pliocene to Quaternary (Silcretes, ferricretes, Willawortina formation).....	26
2.2 Background information on the mineralisation and previous work.....	27
2.2.1 Geometry, relationship to formations, regional faults.....	27
2.2.2 Mineralogy and geochemistry.....	28
2.2.3 Genesis.....	28
3 Methodology and information on WC2.....	29
4 The heavy mineral assemblages.....	32
4.1 Detrital minerals populations.....	32
4.2 Trace element chemistry of zircon.....	36
4.3 Zircon typology and regional correlations.....	39
4.3.1 “SB” zircon typology.....	39
4.3.2 “FMC” zircon typology.....	39
4.3.3 “WC2-63” zircon typology.....	39
4.4 U-Pb zircon data.....	44
4.4.1 U-Pb ages of “FMC” zircons.....	44
4.4.1 U-Pb ages of Beverley Sands zircons (WC2-63).....	44
5 Authigenic mineralogy.....	47
5.1 Native metals.....	47
5.1.1 Native copper and copper-zinc alloys.....	47

5.1.2	Native lead (Pb).....	48
5.2	The “uraniferous nodules” mineralisation.....	51
5.2.1	Introduction.....	51
5.2.2	Background data on coffinite.....	51
5.2.3	Chemical composition and morphology of the uraniferous nodules.....	51
5.2.4	U-Pb geochronology and geochemistry on coffinite / uraninite	56
5.3	Sulfides.....	58
5.3.1	Pyrite and marcasite.....	58
5.3.2	Sphalerite.....	58
5.3.3	Chalcopyrite.....	58
5.3.4	Sulphur isotopes.....	58
5.4	Sulfates: gypsum, barite, alunite.....	59
5.4.1	Repartition of sulfates.....	59
5.4.2	Sulphur isotopes.....	60
5.5	Vanadates: Carnotite, $K_2(UO_2)_2(V_2O_8) \cdot 1-3H_2O$	60
5.5.1	Chemistry and mode of occurrence.....	61
5.5.2	U-Pb-Pa-Th geochronology.....	61
5.5	Carbonates.....	62
6	Whole-rock geochemistry.....	63
6.1	Major elements and general mineralogy.....	63
6.2	Trace elements and geochemistry of mineralization.....	63
6.3	REE patterns.....	63
7	Interpretation of data.....	68
7.1	Paleoenvironment and origin of the Beverley sediments.....	68
7.1.1	Alpha mudstone unit.....	68
7.1.2	Beverley sands unit.....	68
7.1.3	Beverley clay unit.....	69
7.1.4	Willawortina Formation.....	69
7.2	Age constraints and timing of the mineralisation.....	70
7.3	Reconstitution of the physico-chemical conditions during mineralizing time.....	71
7.3.1	Chemistry of groundwaters.....	71
7.3.2	The reduced mineralisation.....	71
7.3.3	The oxidized mineralisation and alteration.....	72
7.3.4	The REE geochemistry.....	74
7.4	The source(s) of uranium.....	77
7.4.1	Potential uranium reservoirs identification.....	77
7.4.2	Mass balance calculation for uranium reservoirs.....	77
7.5	The path of the mineralised fluids.....	80
8	Conclusions.....	81
8.1	Implications for new uranium deposits findings and recommendations.....	81

PART TWO – Metallogeny of uranium and thorium in the Mount Painter Domain	
(North Flinders Ranges, South Australia).....83	
1	Introduction84
2	Geology & metallogeny of the Mount Painter Domain.....85
2.1	The Proterozoic MPD basement and cover.....85
2.1.1	Volcano-sedimentary successions..... 85
2.1.2	Granites, granitoids and volcanics.....85
2.1.3	Mafic intrusions, volcanism and Neoproterozoic cover.....89
2.2	The Paleozoic.....89
2.2.1	Delamerian orogeny (Cambro-Ordovician).....89
2.2.2	Late-Ordovician thermal event.....89
2.2.3	Post-Ordovician tectonics and hydrothermalism.....90
2.3	Mineralisations and previous exploration overview.....92
2.3.1	Mineralisations in pegmatites & granitic rocks.....93
2.3.2	Metasomatic mineralisations (gneisses and skarns).....94
2.3.3	Breccia-hosted mineralisations.....94
2.3.4	Metamorphism-related REE mineralisations.....94
2.3.4	Other types of U-REE mineralisations.....94
3	Regional geochemistry of the MPD96
3.1	Exploration data: radiometrics and rock analyses.....96
3.2	Sample location.....104
3.3	Uranium and thorium in granites: a review.....105
3.4	Granites suites in the MPD: a review.....108
4	Mineralogy and petrology.....109
4.1	The Yerila granite complex, Mount Babbage Inlier.....109
4.1.1	The Yerila granite.....110
4.1.2	The Paleozoic intrusives.....111
4.1.3	Heavy minerals fro stream sediments.....112
4.1.4	Mafic dikes.....114
4.1.5	Mineral and rock chemistry.....114
4.2	The allanite skarns from the Brindana Gorge area.....125
4.2.1	Mineral Chemistry.....126
4.3	The Mawson Plateau watershed.....129
4.3.1	Mineralogy.....129
4.3.2	Mineral chemistry.....129
4.4	Mt Gee - Radium Ridge area mineralisations.....130
4.4.1	The hematite-monzite bodies at Radium Ridge Nr.2 Workings.....130
4.4.2	Migmatitic gneisses from the Radium Creek Metamorphics, Nr.8 Workings crest.....130
4.4.3	The “radioactive ilmenite” from the Nr.10 Workings, Mt Gee West.....131
4.4.4	Corundum-sapphirine-biotite-phlogopite schists.....131
4.5	The Mt Paralana Plateau – Hidden Valley Complex.....132
4.5.1	Geology of the Hidden Valley Complex (HVC).....132
4.5.2	Geology of the migmatitic gneisses and schists Unit.....136
4.5.3	Complimentary data from the Bottleneck Creek sediments.....137
4.5.4	Geology of the Brannerite Hill.....137
4.5.5	Uranium, thorium and REE mineralisations.....137

5	Geochronology	146
5.1	Regional data.....	146
5.2	The Four Mile Creek zircons- British Empire granite/migmatites.....	147
5.3	The Mawson Plateau watershed	147
5.4	The Yerila granite area.....	147
5.5	The allanite skarns from the Brindana Gorge	148
5.6	The Hidden Valley Complex.....	149
5.7	Mt Gee - Radium Ridge to Hidden Valley mineralisations	149
6	Mobility and timing of U, Th and REE.....	162
6.1	Petrogenesis of the U- and Th-rich Yerila granite and related rocks in the MPD.....	162
6.2	New geochronological framework in the MPD and HSFE mobility.....	164
6.2.1	Palaeoproterozoic	164
6.2.2	Mesoproterozoic magmatism and postmagmatic metasomatism.....	164
6.2.3	Neoproterozoic rifting and alkaline metasomatism.....	165
6.2.4	Delamerian Orogeny, metamorphism and migmatitisation.....	165
6.2.5	Palaeozoic magmatism, hydrothermalism, brecciation and exhumation.....	166
6.2.6	Cretaceous-Cenozoic supergene uranium remobilisation.....	167
	GENERAL CONCLUSIONS.....	168
	REFERENCES.....	170
	APPENDIX I to VIII.....	

List of Figures I

Fig. 1:	Hydrologic and topographic map of the North Flinders Ranges.....	15
Fig. 2:	Grid of zircon typology after the Pupin (1980) classification.....	17
Fig. 3:	SEM image of coffinite matrix and corresponding EMPA excitation volumes projected onto the surface..	18
Fig. 4:	Regional geological map of the Mount Painter Domain (MPD) and Paralana High Plains.....	25
Fig. 5:	Regional lithostratigraphy for the Mesozoic and Cainozoic Units.....	26
Fig. 6:	Location map around the Beverley mine in the Paralana High Plains.....	27
Fig. 7:	WC2 log with gamma, uranium grades and heavy minerals assemblage.....	31
Fig. 8:	Sedimentary textures in Beverley Sands.....	33
Fig. 9:	Diagrams of trace elements in the zircons (ICPMS).....	34
Fig. 9 (suite):	Diagrams of trace elements in the zircons (ICPMS).....	35
Fig. 10:	Distribution of zircons in WC2 according to their level and U/Th value.....	37
Fig. 11:	Relationship U/Th ratio and apparent ^{208}Pb - ^{232}Th ages in Beverley zircons.....	38
Fig. 12:	Typical “D” zircons from K-rich granitoids (left) and xenotime crystals from FMC (right).....	40
Fig. 13:	Typology of zircons in WC2-63, FMC and SB.....	41
Fig. 14:	Typology of zircons in FMC divided by age groups (from U-Pb data).....	42
Fig. 15:	U-Pb Concordia diagram of Four Mile Creek zircons (FMC) with 2σ ellipses	43
Fig. 16:	U-Pb Concordia diagram of Beverley sands zircons (WC2-63) with 2σ ellipse	45
Fig. 17:	Pictures of dated zircons from the Beverley Sands (level -124m) with the typology data & U-Pb ages.....	46
Fig. 18:	EMPA analysis of native copper & Cu-Zn alloys from the Beverley Sands (WC2).....	47
Fig. 19:	Native copper grains from the Beverley Sands (WC2).....	48
Fig. 20:	Authigenic mineral inclusion in the Beverley sediments: barite, coffinite, native lead.....	50
Fig. 21:	Coffinite nodules in silt matrix (left) and HM concentrates from the Beverley Sands (right).....	51
Fig. 22:	Coffinite textures revealed by SEM images.....	53
Fig. 23:	EMPA cross-sections of two coffinite nodules	54
Fig. 24:	EMPA Diagrams of coffinite	55
Fig. 25:	Rietveld refinement of X-ray powder diffractogram with coffinite & uraninite.....	56
Fig. 26:	Concordia plot of coffinite nodules (La-ICPMS).....	57
Fig. 27:	Marcasite crystals and twinned “fer-de-lance” couples.....	58
Fig. 28:	Barite crystals in HM concentrate from WC2.....	60
Fig. 29:	Carnotite crystals from the Beverley Sands and clays.....	61
Fig. 30:	Concordia plot of carnotite (La-ICPMS).....	62
Fig. 31:	PAAS-normalised REE spectra for Beverley sediments.....	66
Fig. 32:	PAAS-normalised REE spectra for Beverley coffinite nodules.....	67
Fig. 33:	Polar projection of the southern Gondwana area at ~150 Ma.....	70
Fig. 34:	Log $f\text{O}_2$ (g) vs. pH diagrams for U, Cu, Pb, Zn, Fe and Al	73
Fig. 35:	Saturation index as a function of pH for the Beverley water	74
Fig. 36:	Thorium map of the Lake Callabonna – Mount Painter Domain.....	75
Fig. 37:	Cross-section and perspective projection of the Paralana High Plains to the MPD.....	79

List of Figures II

Fig. 1: Simplified tectonic map of Australia with major Proterozoic and Archaean geological provinces.....	85
Fig. 2: Tectonic map of the Mount Painter Province and subdivisions.....	87
Fig. 3: Synoptic representation of the felsic igneous rocks and migmatitic rocks of the MPD	88
Fig. 4: Synoptic representation of thermochronological data in the MPD	91
Fig. 5: U-REE-Th mineral occurrences of the MPD and region.....	95
Fig. 6a: Sodium whole-rock data in the MPD.....	96
Fig. 6b: Thorium whole-rock data in the MPD.....	97
Fig. 6c: Uranium whole-rock data in the MPD.....	97
Fig. 6d: Copper whole-rock data in the MPD.....	98
Fig. 6e: Cerium whole-rock data in the MPD.....	98
Fig. 6f: Cadmium whole-rock data in the MPD.....	99
Fig. 6g: Tin whole-rock data in the MPD.....	99
Fig. 6h: Arsenic whole-rock data in the MPD.....	100
Fig. 6i: Gold whole-rock data in the MPD.....	100
Fig. 6j: Lanthanum whole-rock data in the MPD.....	101
Fig. 6k: Niobium whole-rock data in the MPD.....	101
Fig. 7: Thorium radiometric map of the Pre-Mesozoic basement of the MPD region.....	103
Fig. 8: Samples map.....	104
Fig. 9: Uranium versus Thorium in granites and igneous alkaline intrusions devoid of metasomatic overprint....	107
Fig. 10: Geologic map of the studied area in the Mount Babbage Inlier (MBI).....	109
Fig. 11: Polished rock samples of Yerila granite YER-03 and YER5.....	111
Fig. 12: Zircon typology grids for Yerila-Ck and SED-BAD.....	113
Fig. 13: “K”-type zircon from Yerila-Ck and quadratic columbite prism from SED-BAD.....	113
Fig. 14: Chemical representation for amphibole, biotite and ilmenite from YER-03.....	115
Fig. 15: Chemical representation for apatite and titanite from YER-03.....	117
Fig. 16: Chemical Chemistry of allanite in Yerila (YER-03).....	118
Fig. 17: Chemical representation for zircon from YER-03.....	119
Fig. 18: Ternary diagrams for garnets from SED-BAD and SED1 samples.....	122
Fig. 19: Monazite and xenotime chemistry diagrams from SED1, SED-BAD and FMC.....	123
Fig. 20: Cerianite and cerium-rich hollandite group grains from SED-BAD.....	124
Fig. 21: Geological map of the Brindana Gorge and the radiometric “Yerila-like” anomaly.....	127
Fig. 22: Th-U-Ca silicate grains from the skarn JB05-37.....	128
Fig. 23: Geological map of the Paralana Plateau – Hidden Valley Complex regions.....	134
Fig. 24: Geological map of the Brannerite Hill area.....	139
Fig. 25: Geological map of the Southern HVC and the Oppidum Creek gorge	140
Fig. 26: Pictures of the Brannerite Hill and the Oppidum Creek gorge	141
Fig. 27: Geological map of the Hot Springs Creek gorge brannerite mineralisation.....	142
Fig. 28: Mineralisations from the Brannerite Hill – Hidden Valley Complex.....	144
Fig. 29: Pictures of REE mineralisations from the Brannerite Hill – Hidden Valley Complex.....	145

Fig. 30: Electron microprobe cumulative ages for monazites from the MPD.....	151
Fig. 31: Zircons from FMC samples with BEG Ordovician concordant zircons.....	152
Fig. 32: Zircons from the Mawson Plateau creek (SED1).....	153
Fig. 33: U-Pb isotopic data for minerals in the Yerila granite (YER03).....	154
Fig. 34: U-Pb isotopic data for diverse samples from Yerila granite and Terrapinna granite.....	155
Fig. 35: U-Pb isotopic data for minerals in the Yerila granite and intruding amphibolite.....	156
Fig. 36: U-Pb isotopic data for minerals from Allantite Skarn (JB05-37).....	157
Fig. 37: U-Pb isotopic data for rutile from Allantite Skarn (JB05-37).....	158
Fig. 38: U-Pb isotopic data for diverse rocks from Hidden Valley Complex (A).....	159
Fig. 39: U-Pb isotopic data for diverse rocks from Hidden Valley Complex (B).....	160
Fig. 40: U-Pb isotopic data for primary U-rich minerals – HVC – Paralana Plateau – Mt Gee.....	161
Fig. 41: Global comparison between MPD granites with possible Th-U enrichment processes.....	163

List of Tables I

Table 1:	EMPA analytical parameters, analysed elements and standards.....	18
Table 2:	Heavy minerals assemblage in the WC2 drill core.....	30
Table 3:	Heavy minerals assemblage in the FMC sample.....	32
Table 4:	LA-ICPMS U-Pb zircon for WC2-63 (Beverley Sands).....	45
Table 5:	EMPA analyses of native lead particles.....	49
Table 6:	EMPA analyses of Co-rich pyrite cores.....	52
Table 7:	Chemical composition of the WC2 drilling sediments at the Beverley Uranium Mine.....	65
Table 8:	Uranium reservoirs and their possible link to the Beverley Uranium deposit genesis	76
Table 9:	Mass balance calculation and evaluation of the potential uranium reservoirs for Beverley.....	78

List of Tables II

Table 1:	U-Th-REE mineral species reported in the MPD pre-2003.....	93
Table 2:	Granites and alkaline igneous uranium-rich rocks.....	106
Table 3:	Mineralogy of the SED-BAD HM concentrates.....	112
Table 4:	Whole-rock analysis of the hematite-monzazite ore at Nr.2 Workings.....	130
Table 5:	Mafic intrusives in the Hidden Valley Complex region.....	133

List of Appendix

Appendix I	Trace elements in zircons from the WC2 sediments.....	
Appendix II	Uranium, thorium and REE occurrences in the MPD.....	
Appendix III	Whole-rock chemical analyses.....	
Appendix IV	EMPA analyses of the Yerila granite.....	
Appendix V	LA-ICPMS U-Pb isotopic analyses.....	
Appendix VI	Sample location & description	
Appendix VII	EMPA analyses and dating of monazites.....	
Appendix VIII	LA-ICPMS calculations.....	

ABSTRACT

The geological province of the Mount Painter in the North Flinders Ranges (South Australia) is well-known for its uranium mineralisation, and uraniferous granites. The presence in the nearby Cenozoic sediments of the Lake Frome basin of uranium mineralisations (Beverley deposit) and the recent discovery of the Four Mile deposit has triggered the interest of explorers. Based on extensive laser-ablation inductively-coupled-plasma-mass-spectrometry (LA-ICPMS) U-Pb geochronological data and mineralogy of U-Th-bearing minerals, rock geochemistry and petrography, we present a global study on the mobility of U, Th and REE in the Mount Painter Domain, including a detailed reconstitution of the Beverley deposit genesis.

Seven significant stages of U-Th-REE mobility are recognised:

1. The possible presence U-enriched ~1600 Ma lower crust under the MPD
2. Intrusion of two A-type Mesoproterozoic granites suites (~1575, and ~1560 Ma respectively) with high HFSE contents and crustal origin; the porphyritic biotite K-rich highly-enriched Yerila granite belongs to the youngest suite and hosts magmatic allanite-(Ce), potassic-hastingsite, ilmenite, fergusonite-(Y), chevkinite, molybdenite, zircon, uranothorite, uraninite and titanite and fluorite
3. Late-magmatic or post-magmatic metasomatism in the same granites; evidenced by F-rich annite, zircon, Y-bearing Al-F-titanite (< 6 kbar, >400°C), Y-rich fluorapatite, synchysite-(Ce) and fluorite. Early ilmenite, molybdenite, allanite-(Ce) and oligoclase reacted with an alkaline oxidising F-rich melt or fluid. The late-magmatic to post-magmatic metasomatism is also recorded at the intrusion contact in regional rocks, forming allanite-, magnetite-, uranothorite-, zircon- (1501 ± 6 Ma), and uraninite-bearing calcsilicate skarns. The spreading of zircon ages in the Yerila granite (~1565 to ~1521) relates to the mixing of magmatic and metasomatic crystals.
4. the MPD was subject to the Delamerian orogeny and related metamorphism (amphibolite facies); most Mesoproterozoic granitic assemblages present signs of recrystallisation or stress; recrystallisation of monazite-(Ce) and xenotime-(Y) during Paleozoic (Cambrian) (490-495 Ma). U-Th-rich minerals also bear Delamerian ages (polycrase-(Y), euxenite-(Y), davidite-(La) and uraninite).
5. Anatexis of local basement during Ordovician and generation of peraluminous granite (British Empire granite) with low Th/U. The granite is enriched in U and Y. We provide the first robust ages on it: 456 ± 9 and 459 ± 9 Ma on zircon, 453.3 ± 4.6 on xenotime-(Y).
6. Very active hydrothermal/pegmatitic uranium remobilisation along active faults; brannerite-quartz veins formation (367 ± 13 Ma), further signs of remobilisation or hydrothermal event during Permian (284 ± 25 Ma in thorite) and around the Mt Gee (~290 Ma radiogenic gain in davidite) which agrees with the previous data (paleomagnetic ages of 250-300 Ma).
7. Cenozoic supergene uranium remobilisation in MPD and migration of U-rich oxidised groundwaters into the Lake Frome. The uranium is precipitated in the sandy formation of the lake and in the top layer of the underlying organic-matter-rich clays and silts. The micro-environment of reduction efficiently trap U but also REE, fingerprinting the REE-rich MPD granite source. Coffinite and carnotite give concordant Pliocene ages (6.7 to 3.4 Ma).

Provenance studies on the sands hosting the Beverley mineralisations suggest a reworking of Early Cretaceous glacial or glacio-lacustrine sediments originally sourced in Eastern Australia (Lachlan Fold Belt). The youngest recorded zircon (130 Ma) doesn't constrain the sediment age but refines the provenance region (New England Orogen).

DECLARATION

This thesis contains no material which has been accepted for the award of any other degree or diploma in any university and, to the best of my knowledge and belief, contains no material previously published or written by any other person, except where due reference has been made in the text.

I give my consent for this copy of my thesis, when deposited in the University Library, being available for loan and photocopying.

Pierre-Alain Wülser

ACKNOWLEDGMENTS

Arrived to the end of this long adventure, I would like to remember how this all started.

The idea of this PhD research was initiated in 2002 during an animated discussion, after several glasses of red wine at the inauguration of the new mineralogical display of the Musée Cantonal de Géologie de Lausanne. The idea evolved and finally took form a few months later. My passion for uranium minerals ignited when I was told the research could be done on this element, in one of the most uraniumiferous province in the world: the region of the Mount Painter in South Australia.

After five and a half years of perseverance, patience and sometimes discouragement, I would like to thank all those who contributed to this achievement.

To Samantha, my wife, for the patience and love, to have saved me from being expelled from the country when my scholarship ran out, for your unlimited support, thank you so much! A special thank you to my family, for the support and encouragement and visits you gave me during these years.

To Joël Brugger and John Foden, for the supervision and the support during the evolution of this project, the constructive discussions, the patience and the constant “kick” for limiting my exaltations of driving me away from the main research goal. Thank you a lot.

I would like to address a special thank you to the Sprigg family, for access to Arkaroola, providing accommodation and the wonderful scenic flight. Thank you Doug.

Thank you to the Centre d'Analyse Minérale in Lausanne, especially Hans-Rudolf Pfeiffer and Jean-Claude Lavanchy for providing the technical support for analyses and access to the labs; a special thank to Laurent Nicod and Wally Fander, for their precious help in the petrographic preparations and observations. To Yann Lahaye, for the help during my first contact with the LA-ICPMS technique and Olivier Parize, for the precious help given during the core logging, thank you.

I am grateful to the team of the Adelaide Microscopy Centre, especially Angus Netting, Peter Self and John Terlet for their precious help during the hundreds of hours spent at analysing and dating minerals. Thanks a lot.

The first three years of the PhD were financed through IPRS and CRC-LEME scholarships, from which most of the analytical costs were covered. The achievement of this research has been supported by the company Heathgate Resources Pty Ltd, which provided some logistical and financial support during the period 2007-2008. A special thank to Jess Oram and Geoff McConachy.

To my friends, Patrick, Patoche, Julien, Mathieu, Pascal, Camla, Ralf, Michelle and David, thanks a lot for everything and the unforgettable moments spent together during these years.

The providential “silvery bin”, the patient panning of 1800 kilos of dirt, and finally the bloody massive branch sawn during a early morning in Parkside have to be remembered here as the luck and perseverance factors.

GENERAL INTRODUCTION

This research project is centred on uranium metallogeny in the North Flinders Ranges region of South Australia (Fig. 1). South Australia is home to the Olympic Dam deposit, the largest uranium resource in the world. Prior to the discovery of this giant, numerous uranium occurrences were already known in the state. These occurrences were essentially concentrated on or around the outcrops of Proterozoic rocks: the Gawler craton and the Curnamona craton (or province). The North Flinders Ranges form the extremity of a mountain chain which essentially separates the two Proterozoic regions.

The choice to focus on the North Flinders Ranges was made because of its exceptional setting, with a large section of the Mesoproterozoic basement outcropping in a tectonic window: the Mount Painter and Babbage Inliers. These inliers show a large number of uranium occurrences and deposits. The sediments of the basin to the Eastern part of the inliers also host the operating Beverley uranium mine and another deposit discovered in 2005 during the period of this research: the Four Mile uranium deposit.

Another particularity of these inliers is the presence of granites and gneisses with exceptional concentrations of both Th and U. The extreme cases are met in the Yerila granite (116 ppm U and 423 ppm Th) and the Hot Spring Gneiss (75 ppm U, 288 ppm Th) and the concentrations have been considered to have a magmatic origin (Neumann *et al.* 2000).

The research is divided in two parts:

1. the study of the Beverley uranium deposit;
2. the timing and description of uranium mobility in the outcropping basement.

There are a number of research questions that we ask at the beginning of this thesis:

- What is the timing of the Beverley deposit?
- Where is the Beverley uranium coming from?
- How did the exceptional U concentrations in some Mesoproterozoic granites evolve?
- When and under what circumstances did uranium remobilisations occur?

For the purpose of documenting these questions, the following works were conducted: field mapping, sample collecting, heavy mineral separations and studies, U-Th-Pb isotopic measurements for geochronology, geochemical analyses, sedimentary provenance study, petrography and mineralogy.

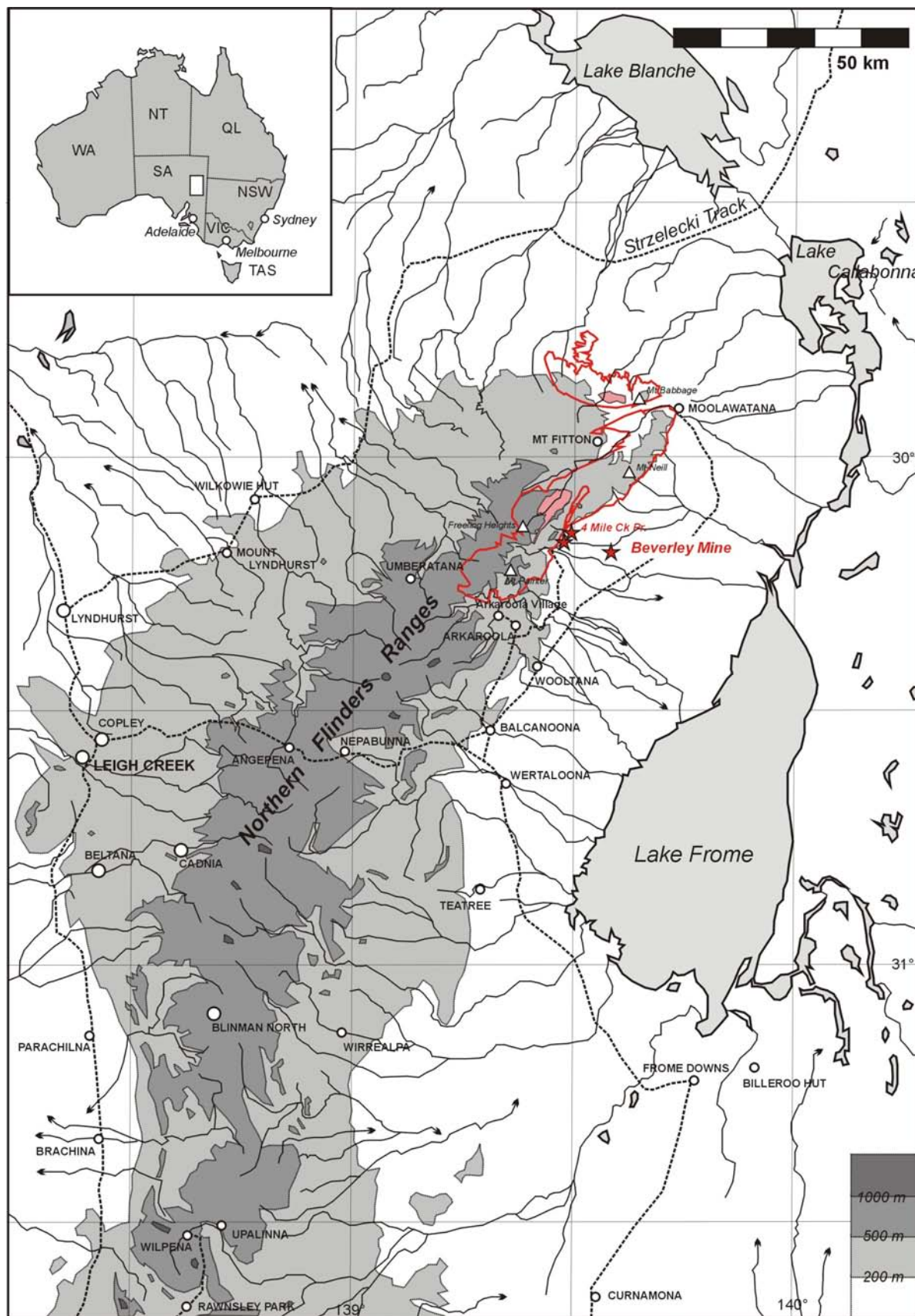


Fig. 1: Hydrologic and topographic map of the North Flinders Ranges.

The Beverley and the 4 Mile uranium deposit are displayed by red stars and the Mount Painter Domain (MPD) is delimited in red. The Palaeozoic granitoids are represented in pink. Almost all the relief forming the Ranges is composed by the Neoproterozoic to Cambrian “Adelaide Geosyncline” formations.

ANALYTICAL TECHNIQUES

A.1 Heavy mineral and sample preparation

Heavy minerals were extracted and concentrated from sediments or crushed rocks by panning and micro-jigging, and then were further separated by permanent magnets. To avoid cross-contamination resulting from the use of heavy liquids and electromagnets, the whole procedure was hand-actioned. However, in the case of cored sediments, a possible contamination due to the drilling process and the transportation to the storage is inevitable.

The washing of sediments was conducted in soapy water to individualise all particles and avoid grains to float in presence of organic matter or drilling grease. The recovered HMs concentrates were extracted from the pan after the obtention of a fraction of HM estimated to be more than 3.0 g/cm³ in density. Then, the HM's were washed with pure water and alcohol to be finally dried on a paper sheet. The sand-silt fractions were separated by a strong hand magnet (Fe-Nd-B) into three fractions: MM (ferromagnetic), SM (paramagnetic) and NM (non-magnetic). The pulling force of the permanent magnet against its surface was equivalent to 1.35 Ampere intensity on a Frantz Isodynamic Separator (calibrated on 150 µm fraction). The NM and the SM fractions have been then jigged in a small rigid pan in order to separate them into an approximate <4.0 g/cm³ and >4.0 g/cm³ fractions containing an almost pure concentrate of zircon-rutile-corundum.

Final concentrates were examined under a binocular microscope and hand-picked for typology (zircon), further analysis or digital photography. Minerals selected for chemical analysis, ICPMS dating or electron microscope study were mounted in epoxy resin discs and polished. The HM concentrates were examined for diverse grain counting to determine the relative proportion of each mineral species. Typically, a “rutile/ (rutile + zircon)” index was determined by counting, similar counting were applied to other minerals.

Impregnated chips of sediments were dried and directly mounted in epoxy for electron microscope observations. Polishing of clays and mudstone sections was conducted without any liquid to avoid desegregation or mineral leaching.

A.2 Zircon typology and morphology: principles

Zircon typology or morphology has been used as a tool to distinguish the nature of granites (Pupin, 1980) and to distinguish magmatic and inherited zircons in igneous rocks (Klötzli et al., 2001). Surface textures also provide information about the provenance of the grains (Cardona et al., 2005), and a combination of dating and typology can determine sedimentary provenances with better precision (Willner et al., 2003). The principle of zircon typology is based upon the relative abundance of prisms and pyramids. Crystal forms have been divided into 64 main subtypes, corresponding to a unique combination of these crystal faces. The zircon types are reported in a square “chessboard-like” chart, with colour filling proportional to the percentage of appearance (Fig. 2). Placing a whole sedimentary population permits to distinguish clusters of different origins. The distribution of the zircon subtypes in granitic rocks shows specific populations, which can be divided into eight main genetic subgroups. The relative abundance of the prisms (100) and (110) also documents the temperature of crystallization. Application to sedimentary zircon is however more complex because of all the possible mixing present and the proportion of “undetermined” types grains as a consequence of the mechanical wearing of crystal faces. This later morphological type can dominate the others. Observations are generally made on pure zircons fractions, either by SEM examination for small crystals or under microscope for zircons >150 µm. One advantage of using the optical microscope instead of SEM is the possibility of picking a grain and to rotate it attached to the end of a needle.

A.3 Chemical and isotopic composition analysis

Chemical analyses were conducted either by semi-quantitative Energy-Dispersive Spectroscopy (EDS) on an electron microscope, or Wave-Dispersive Spectroscopy (WDS) on an electron microprobe.

A.3.1 Backscattered Scanning Electron microscope study

Heavy minerals generally contain at least one element whose atomic mass is higher than the average surrounding common silicate minerals. The brightness of Backscattered electron (BSE) images is proportional to the average atomic mass at the scanned spot. It becomes easy to detect small grains of HM minerals or mineralised coatings on large surface of rock/grains sections or mounts by varying the contrast of the image. Identification of the mineral is also possible synchronously to the observation via EDS spectroscopy. This technique was especially useful for recognition of columbite and tantalite in the ilmenite concentrates from the sediments.

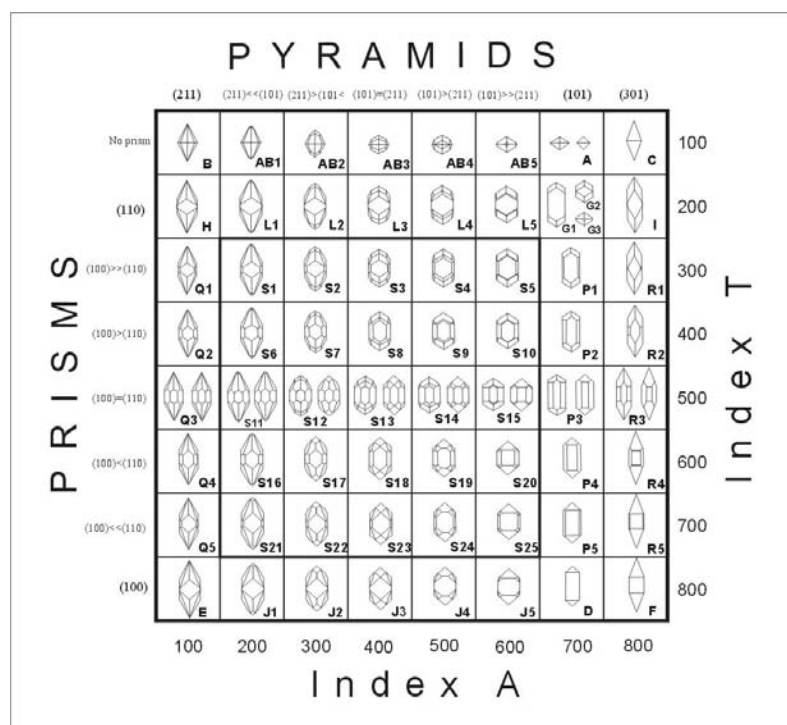


Fig. 2: Grid of zircon typology after the Pupin (1980) classification

Each unique combination of prisms and pyramids correspond to a specific type, which is denominated by a letter and a number. Exceptions are zircons presenting “end-member” typologies (types A, B, C, D, E, F, G, H, I). D-type with (301) pyramids are called K and are reported with D. T-types with presence of (301) pyramids are called T (T1-T5) and are reported with P types.

A.3.2 Electron microprobe analysis

Quantitative compositional analyses of HM were made using a CAMECA SX51 electron microprobe at the Microscopy Centre of the University of Adelaide on carbon-coated epoxy resin blocks. Special care was taken for native metals analysis to avoid any surface oxidation. Sections were re-polished and coated a few hours before analysis. The Astimex Scientific Ltd standards were used for element calibration. However, some matrix are totally different and this may have caused some imprecision in the results. Analytical conditions were 1 μm , 20 nA and 20 kV. The analysed elements and used standards are reported in Table 1. Counting times varied between 10 and 60 seconds, depending upon the required detection limits.

The porous nature of some U-rich minerals like the coffinite nodules or metamict uranothorite leads to low analytical sums and relatively large excitation volumes. In this case, analyses are more semi-quantitative because the standards used have a different matrix and elemental density. The profiles across nodules show irregularities and quartz inclusions. The low totals of oxides are related to both porosity and water content. SEM pictures have been used to understand the effect of an electron beam in the coffinite samples (Fig. 3). The excitation volume resulting from the 20 kV accelerating voltage, with a focused beam (1 μm), has a varying radius from 3.1 to 1.7 μm (Potts, 1987), depending whether the matrix is porous, silica- or uranium-rich. As a result, measurements in the WDS crystals are systematically taking into account some pores which are empty, or containing clay or amorphous silica. For more information on the problems met during coffinite analysis, the reader is referred to the exhaustive review published recently by Förster (2006).

A.3.3 Sulphide isotopes determination

Analyses have been performed at the Stable Isotope Laboratory of the University of Lausanne (Switzerland), using the on-line elemental analyser (Carlo Erba 1108) –continuous flow-isotope ratio mass spectrometer (Finnigan Mat Delta S). The analytical uncertainty (2σ) was 0.2 ‰, with the exception of the pyrite inclusions in coffinite: 0.3 ‰. The data are reported as per mil (‰) deviations relative to the Canyon Diablo Troilite (CDT) standard. Analyses were repeated 2-3 times when enough material was available and alternated regularly with international sulphide and sulphate standards.

Coffinite, metals & sulphide, carnotite				Zircon, apatite & xenotime			
20kV, 20nA, spot size 1 μ m				20kV, 20nA, spot size 1 μ m			
Line.	Crystal	Standard	Interf. cor.	Line	Crystal	Standard	Interf. cor.
MgK α	TAP	<i>Biotite</i>	—	FeK α	LIF	<i>Almandine</i>	—
AlK α	TAP	<i>Biotite</i>	—	ErM α	TAP	<i>Erbium metal</i>	—
SiK α	TAP	<i>Biotite</i>	—	YbM α	TAP	<i>synthetic YbF₃</i>	—
PK α	PET	<i>Apatite</i>	Y	HfM α	TAP	<i>Cubic Zirconia</i>	—
SK α	PET	<i>Marcasite</i>	—	CaK α	PET	<i>Almandine</i>	—
KK β	PET	<i>Biotite</i>	U	ZrL α	PET	<i>Cubic Zirconia</i>	—
CaK α	PET	<i>Apatite</i>	—	YL α	PET	<i>Cubic Zirconia</i>	—
VK α	LIF	<i>Rutile</i>	Ti	PbM α	PET	<i>Crocoite</i>	—
FeK α	LIF	<i>Marcasite</i>	—	PK α	PET	<i>Apatite</i>	Y
CoK α	LIF	<i>Cobaltite</i>	—	ThM α	PET	<i>Monazite</i>	—
NiK α	LIF	<i>Pentlandite</i>	—	UM β	PET	<i>Uranium metal</i>	—
CuK α	LIF	<i>Copper</i>	Ba	AlK α	TAP	<i>Almandine</i>	—
ZnK α	LIF	<i>Zinc</i>	U	SiK α	TAP	<i>Olivine</i>	—
AsL α	TAP	<i>Cobaltite</i>	—	All standards used from Astimex Scientific Ltd Sections METM25-44, REEM25-15, MINM25-53. Variable acquisition time on peak and background CAMECA SX51, Adelaide Microscopy Centre			
SeL α	TAP	<i>Selenium</i>	—				
MoL α	PET	<i>Molybdenite</i>	—				
PdL α	PET	<i>Palladium</i>	—				
CsL α	PET	<i>Pollucite</i>	—				
BaL α	PET	<i>Barite</i>	Cu				
PbM α	PET	<i>Lead</i>	—				
UM α	PET	<i>Uranium</i>	—				

Table 1: EMPA analytical parameters, analysed elements and standards

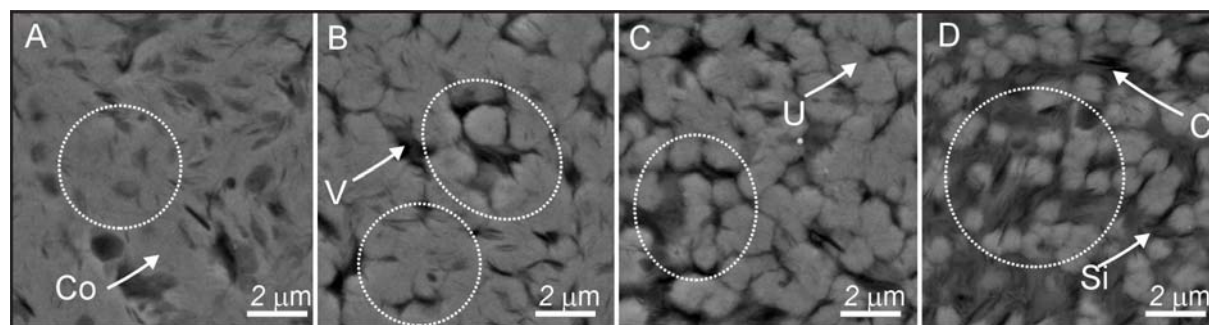


Fig. 3: SEM image of coffinite matrix and corresponding EMPA excitation volumes projected onto the surface.

Electron penetrations after Potts (1987). The four different textures are: A) dense coffinite-amorphous silica; B) dense coffinite-uraninite particles with porosity and small amount of clay minerals; C) same as B with more porosity and clays; D) small (<1 μ m) uraninite-coffinite particles within an amorphous silica-clay matrix. Legend: V=cavities, Co=coffinite, U=uraninite-coffinite dense spot, Si=amorphous silica, Cl=clay. Analytical conditions: 20 kV, 20 nA, excitation volumes: $r = 1.7 - 3.1 \mu\text{m}$

A.3.4 U-Pb dating by laser-ablation ICPMS

Measurements were conducted on a LA-ICPMS in Adelaide Microscopy Centre. The detailed technique and procedure for zircon analysis can be found in Reid *et al.*, (2006). We will however give a detailed procedure of the entire acquisition and data treatment. The ablation is performed using a New Wave 213 nm Nd:YAG laser. The ablated holes measure 40 μ m in diameter and 40-50 μ m in depth. The ablated material is then carried by an Ar-He gas medium into the ICPMS (Agilent 7500 quadrupole plasma mass spectrometer). The plasma operates at $\sim 6725^\circ\text{C}$. The following isotopes were measured: ^{204}Pb , ^{206}Pb , ^{207}Pb , ^{208}Pb , ^{232}Th , ^{238}U with respective dwell times: 10, 15, 30, 10, 10 and 15ms. Background was measured for the first 60s, followed by 120s of ablation. The procedure included a sequence of four standards (red zircon GJ), a series of ten unknowns, an in-door zircon standard (BJWP-1) at ~ 720 Ma to check the accuracy and a final set of four GJ standards.

Raw data is then treated and corrected for fractionation and ratio calculation using the online software GLITTER (van Achterbergh *et al.*, 1999). ^{235}U is calculated using the natural isotopic ratio for uranium: $^{235}\text{U} = ^{238}\text{U}/137.88$. A representative portion of the signal is selected for both standards and unknowns, allowing calculating the fractionation patterns of the diverse measured isotopes along a linear regression between the two sets of GJ

standards. The GLITTER program then delivers the isotopic ratios, $^{207}\text{Pb}/^{235}\text{U}$, $^{206}\text{Pb}/^{238}\text{U}$, $^{207}\text{Pb}/^{206}\text{Pb}$ and $^{208}\text{Pb}/^{232}\text{Th}$ with associated errors, as well as integrated raw counts (background subtracted) for all the measured isotopes. The determination of ^{204}Pb by ICPMS is problematic because this isotope is affected by isobaric overlap with ^{204}Hg , which is present in trace in the argon used as carrier gas. There is a technique using mathematical calculations to correct the presence of common Pb in the analysis without measuring ^{204}Pb (Andersen, 2002). However this method requires a good knowledge of the age of the lead loss. Another way to improve the quality of ^{204}Pb signal is to efficiently trap the ^{204}Hg from the gas using in-line gold traps on the way of the gas carrier line. A perfect correction can be made when measuring another Hg isotope (^{201}Hg) to deduce the exact amount of ^{204}Hg in the “204” signal (Storey et al., 2006); gold traps was evaluated to reduce the ^{204}Hg signals by 70%. Such device has also been setup on the LA-ICPMS used at the Adelaide Microscopy Centre.

The GJ standard used for calibration is a gem quality red zircon with slightly discordant ages: 608.5 ± 0.4 Ma for $^{207}\text{Pb}/^{206}\text{Pb}$, 600.7 Ma for $^{206}\text{Pb}/^{238}\text{U}$ is and 602.2 Ma for $^{207}\text{Pb}/^{235}\text{U}$ (Jackson *et al.*, 2004). The composition of GJ was also used for the uranium and thorium determination: 291.15 ppm U and 11.2 ppm Th. GJ zircon is showing undetectable level of ^{204}Pb with the current LA-ICPMS setting; the reported TIMS values in Jackson et al. (2004) are extremely low: ~ 4 ppb of common Pb corresponding to < 1 cps ^{204}Pb on the used ICPMS.

Use of the gold trap results in low ^{204}Hg background (mean “204” channel on background is 0 or 100 counts). With the extremely low ^{204}Pb content of GJ, measured counts on GJ are similar to background. The mean raw cps minus background measurement of the 204 channel on the GJ standard was defined over the entire dataset acquired in 2006: $20.5 \pm 9.1(1\sigma)$ cps, defining a (3σ) interval between 0.0 and 48 cps. The assumption is made that the GJ zircon represents an almost ^{204}Pb -free ablation blank and any 204 signal > 50 cps represents a measured contribution from ^{204}Pb . Analyses showing 100 cps+ of ^{204}Pb have generally been therefore corrected for common lead.

Common lead correction has been applied using the composition of the global second-stage Pb reservoir of Stacey & Kramer (1975). The lead composition was calculated for each sample using the fractionation parameters (yield factor in GLITTER) generated between ^{208}Pb , ^{207}Pb and ^{206}Pb . Because GLITTER cannot generate isotopic ratio comprising ^{204}Pb , we assume the fractionation between $^{208}\text{Pb}/^{206}\text{Pb}$ is identical to between $^{206}\text{Pb}/^{204}\text{Pb}$.

Each correction is checked individually to detect any problem (lead loss, uranium gain, inheritance, etc.). Also, for mineral devoid of ^{232}Th (rutile, carnotite), the lead correction is made by minimising ^{208}Pb . All ages are reported with (2σ) errors unless specified. Calculations and assumptions used for the corrections are reported in Appendix VIII.

A.3.5 Whole-rock analysis: Fe^{2+} determination & XRF analysis

Rock or sediments chips were crushed finely and prepared for the XRF, ICPMS and ferrous iron analyses. XRF measurements were conducted on a Philips PW2400 spectrometer at the Centre d'Analyse Minérale at the University of Lausanne (CAM). Samples were prepared as melted lithium tetraborate glass discs for major elements and pressed pellets for minor and trace elements measurements. Powders were kept in oven at 110 °C for 24 hours prior to preparations and weighting. Carbon analysis was not performed on samples but organic matter was observed in some of the acid dissolution residues. S was determined on the pressed pellets using the XRF UNIQUANT setting as well as for uranium in the samples that were out of the calibration. Ferrous iron was determined quantitatively by spectrophotometry using the Wilson's modified method (Wilson, 1960). A fraction of rock powder was dissolved in a H_2SO_4 -HF mixture. Solutions were neutralised and buffered with H_3BO_4 , and Fe^{2+} was complexed with 2,2'-bipyridine; the solutions were measured in the maximum range of absorption of the Fe^{2+} complex and FeO (wt-%) calculated using a linear calibration of five rock standards and a blank.

A.3.6 Trace element analysis by LA-ICPMS

The rare earth elements and other traces have been determined by LA-ICPMS on the glass discs. Analyses were performed at the Institut de Minéralogie et Géochimie (University of Lausanne) with an EXCIMER Laser (193 nm) coupled to an ICP-MS Perkin-Elmer ELAN 6100 DRC. Incomplete incorporation of powders into the glass can produce a low content for some trace elements and we carefully checked the quality of the glass discs under microscope to check the absence of inclusions (see section 3.3.5.) The total analytical sums for XRF-FeO are between 99.26 and 99.84 %, monitoring the quality of the work. A simple way to check if the refractory minerals are properly incorporated in the glass is to compare the XRF and the ICPMS values on Zr, Nb or Th: the maximum difference found was $\pm 24\%$ difference. This value is acceptable in order to affirm that zircon (heavy REE main host) was homogeneously incorporated in the glass matrix.

Trace elements in zircon has also been analysed using LA- ICPMS and calibrated using glass standards (NIST 610 glass, 91500 zircon). The following isotopes have been analysed: ^{29}Si , ^{31}P , ^{44}Ca , ^{45}Sc , ^{48}Ti , ^{51}V , ^{55}Mn , ^{57}Fe , ^{63}Cu , ^{66}Zn , ^{69}Ga , ^{77}Se , ^{88}Sr , ^{89}Y , ^{91}Zr , ^{93}Nb , ^{95}Mo , ^{118}Sn , ^{121}Sb , ^{138}Ba , ^{139}La , ^{140}Ce , ^{141}Pr , ^{146}Nd , ^{147}Sm , ^{151}Eu , ^{158}Gd , ^{159}Tb , ^{161}Dy , ^{165}Ho , ^{167}Er , ^{169}Tm , ^{172}Yb , ^{175}Lu , ^{178}Hf , ^{181}Ta , ^{182}W , ^{185}Re , ^{208}Pb , ^{232}Th and ^{238}U . ^{29}Si was used as an internal standard. Calibration problems have been met with the zircons containing a high concentration of heavy rare earths, leading to saturation in Y, Yb and Er. Analyses were performed at the Institute für Mineralogie (J.W. Goethe-Universität,

Frankfurt), using a Merchantek LUV213 petrographic ultraviolet Nd-YAG laser microprobe coupled with a Finnigan MAT ELEMENT II high-resolution ICP double-focusing mass spectrometer.